


# Watershed phenomena during extracorporeal life support and their clinical impact: a systematic *in vitro* investigation

Johannes Gehron<sup>1\*</sup> , Maximilian Schuster<sup>1</sup>, Florian Rindler<sup>1</sup>, Markus Bongert<sup>2</sup>, Andreas Böning<sup>1</sup>, Gabriele Krombach<sup>3</sup>, Martin Fiebich<sup>4</sup>, Philippe Grieshaber<sup>1</sup> and EMPACS (Exploration of the mixing phenomena during interaction of internal and external circulations) study group

<sup>1</sup>Department of Adult and Pediatric Cardiovascular Surgery, University Hospital Giessen, Rudolf-Buchheim-Str. 7, 35392, Giessen, Germany; <sup>2</sup>Research Center for Biomedical Technology (BMT), University of Applied Sciences and Arts, Dortmund, Germany; <sup>3</sup>Department of Diagnostic and Interventional Radiology, University Hospital Giessen, Giessen, Germany; <sup>4</sup>Division of Life Science Engineering, University of Applied Sciences, Giessen, Germany

## Abstract

**Aims** Extracorporeal life support (ECLS) during acute cardiac failure restores haemodynamic stability and provides life-saving cardiopulmonary support. Unfortunately, all common cannulation strategies and remaining pulmonary blood flow increase left-ventricular afterload and may favour pulmonary congestion. The resulting disturbed pulmonary gas exchange and a residual left-ventricular action can contribute to an inhomogeneous distribution of oxygenated blood into end organs. These complex flow interactions between native and artificial circulation cannot be investigated at the bedside: only an *in vitro* simulation can reveal the underlying activities. Using an *in vitro* mock circulation loop, we systematically investigated the impact of heart failure, extracorporeal support, and cannulation routes on the formation of flow phenomena and flow distribution in the arterial tree.

**Methods and results** The mock circulation loop consisted of two flexible life-sized vascular models (aorta and vena cava) driven by two paracorporeal assist devices, resistance elements, and compliance reservoirs to mimic the circulatory system. Several large-bore antegrade and retrograde access ports allowed connection to an ECLS system for extracorporeal support. With four degrees of extracorporeal support—that for cardiac failure, early recovery, late recovery, and weaning—we investigated aortic blood flow velocity, blood flow, and mixing zones using colour-coded Doppler ultrasound in the aorta and its corresponding branches. Full retrograde extracorporeal support (3–4 L/min) perfused major portions of the aorta but did not reach the supra-aortic branches and ascending aorta, resulting in an area in the thoracic aorta demonstrating nearly stagnant blood flow velocities during cardiogenic shock and early recovery ( $0 \pm 4$  cm/s;  $-10 \pm 15$  cm/s, respectively) confined by two watersheds at the aortic isthmus and renal artery origin. Even increased ECLS flow was unable to shift the watershed towards the aortic arch. Antegrade support resulted in homogeneous flow distribution during all stages of cardiac failure but created a markedly negative flow vector in the ascending aorta during cardiogenic shock and early recovery with increased afterload.

**Conclusions** Our systematic fluid-mechanical analysis confirms the clinical assumption that despite restoring haemodynamic stability, extracorporeal support generates an inhomogeneous distribution of oxygenated blood with an inadequate supply to end organs and increased left-ventricular afterload with absent ventricular unloading. End-organ supply may be monitored by near-infrared spectroscopy, but an obviously non-controllable watershed emphasizes the need for additional measures: pre-pulmonary oxygenation with a veno-arterial-venous ECLS configuration can allow a transpulmonary passage of oxygenated blood, providing improved end-organ supply.

**Keywords** Acute heart failure; Circulation; Extracorporeal life support; Cannulation; Fluid-mechanical interaction; Watershed phenomena

Received: 6 February 2020; Revised: 13 April 2020; Accepted: 20 April 2020

\*Correspondence to: Johannes Gehron, Department of Adult and Pediatric Cardiovascular Surgery, University Hospital Giessen, Rudolf-Buchheim-Str. 7, 35392 Giessen, Germany. Email: johannes.gehron@chiru.med.uni-giessen.de

## Introduction

Extracorporeal life support (ECLS) during acute cardiac failure provides life-saving cardiopulmonary support and restores haemodynamic stability. Various vascular access routes, including femoral, subclavian, and direct central cannulation, can be used to initiate this support.<sup>1</sup> Because ECLS initially maintains nearly the entire cardiac output (CO), it may be assumed that the extracorporeal flow is homogeneously distributed within the arterial tree to reach all end organs. However, in most patients on ECLS, the left ventricle maintains some residual output and consequently delivers an antegrade blood flow through the aortic valve towards the systemic circulation.<sup>2</sup> In all cannulation scenarios, the ECLS flow increases the cardiac afterload and is opposed to the antegrade native CO. Despite a normal and non-elevated blood pressure, this retrograde flow vector may increase cardiac afterload, lead to left-ventricular distention, and cause pulmonary oedema.<sup>3,4</sup> Tepper notes that pulmonary recovery begins, at the earliest, 48 h after the implantation of ECLS and the formation of pulmonary oedema.<sup>5</sup> Thus, the compromised pulmonary function may cause the ejection of desaturated blood from the left ventricle for an unknown period. The antegradely flowing and likely hypoxic blood will then collide with the fully saturated retrogradely flowing ECLS blood at varying locations within the aorta. This so-called watershed phenomenon may pose a risk of hypoxaemia to the coronary and cerebral circulation because of the mixing zone, and therefore, the area of deoxygenated blood is unpredictable.<sup>2</sup> A residual pulse pressure, blood gas analyses from different peripheral arteries (e.g. radial and femoral arteries), and near-infrared spectroscopy can serve as surrogate parameters for the localization of the watershed and the resultant end-organ oxygen supply.<sup>6</sup>

Several animal studies and clinical case series have investigated this complex watershed phenomenon. Several decades ago, animal experiments showed that extracorporeal support led to an inhomogeneous distribution of arterialized blood within the arterial tree, which may not reach the brain and the coronaries.<sup>7,8</sup> Although central arterial cannulation caused higher cerebral tissue oxygenation, coronary blood flow still varied with different central cannulation sites, such as the ascending aorta or the brachiocephalic trunk.<sup>9,10</sup> Despite a dependency on the cannulation site, the coronary flow appears to be predominantly driven by left-ventricular action.<sup>11,12</sup> Clinicians have also confirmed the inhomogeneous flow distribution of arterial ECLS flow in patients requiring extracorporeal support by blood gas results and especially by tomography scans with an inhomogeneous contrast agent enhancement within the arterial tree.<sup>13–17</sup>

In conclusion, the watershed phenomenon seems to be inherently connected to ECLS, but it has not yet been investigated systematically. Despite consistent experimental and clinical data, we are still unable to describe how flow vectors, residual left-ventricular function, pulse pressure, and cannulation site influence the formation, location, and potential extent of the watershed phenomenon. These intricately connected flow interactions are not accessible to systematic *in vivo* bedside investigations.

This study systematically investigates the impact of continuously adjustable stages of heart failure, extracorporeal support, and cannulation sites on the formation of the watershed phenomenon in the major arterial tree with an *in vitro* mock circulation loop (MCL) with preserved anatomical structures.

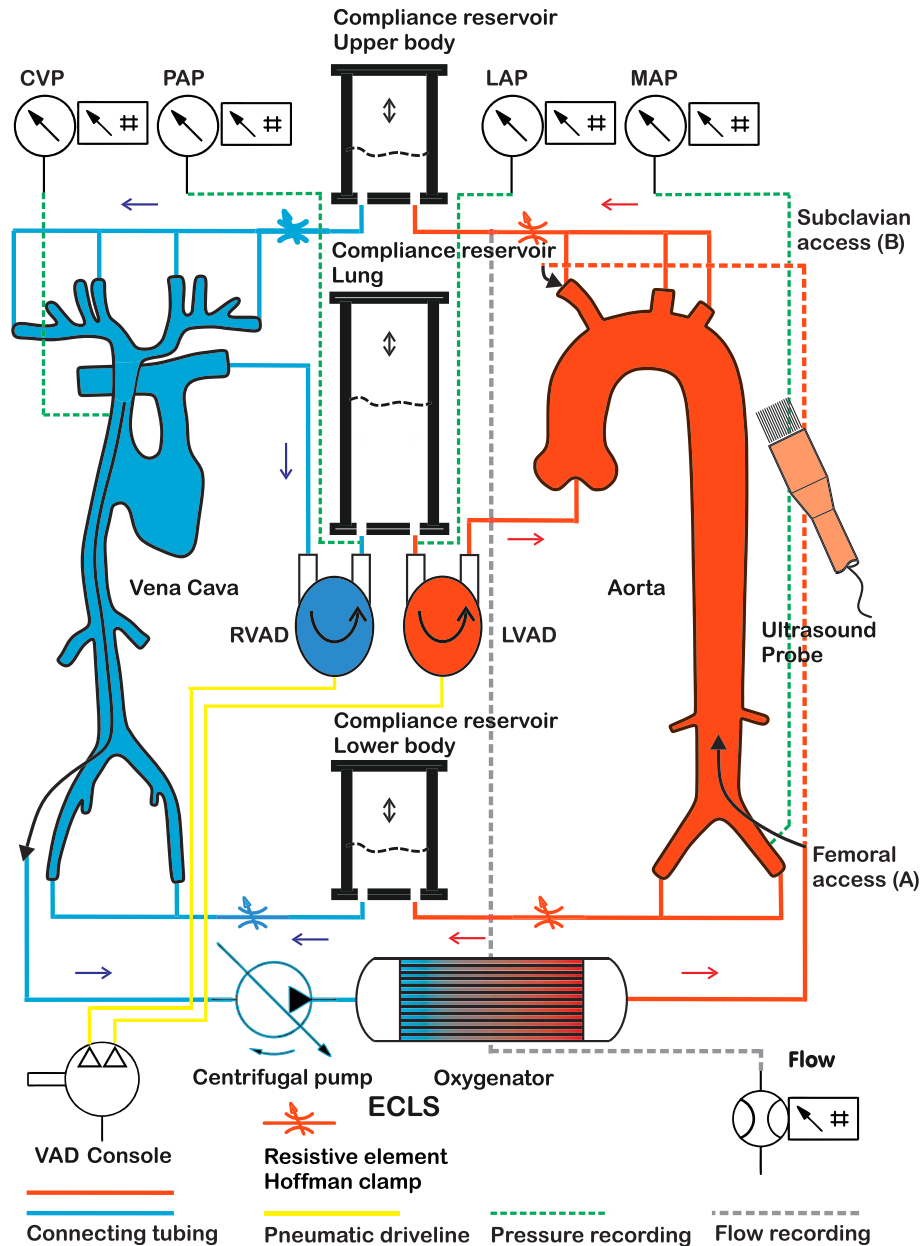
## Methods

### Experimental mock circulation loop design and use

The experimental investigation was conducted using a recently developed life-sized hydraulic MCL that was described previously.<sup>18</sup> Briefly, we mounted two life-sized silicon-based vascular models (aorta, vena cava) (AM00V01 and VCH00V01, respectively; United Biologics, Santa Ana, USA) in a waterproof polyvinylchloride (PVC) housing (volume 180 L; 100 × 60 × 30 cm). The vascular models mimicked the human anatomy in its compliance, elasticity, and size.<sup>19,20</sup> Left and right ventricular functions were established with two paracorporeal pneumatic assist devices with continuously adjustable driving and suction pressure, systolic time, and frequency (HIA-VAD-60 mL; MEDOS, Stolberg, Germany). Both devices were connected in series to the silicone ventricles within the PVC housing (*Figure 1*).

To avoid any aortic regurgitation, we implanted a self-expandable bovine pericardium-based aortic valve prosthesis mounted on a nitinol stent (29 mm, CoreValve Evolute R, Medtronic, Luxembourg) into the aortic root of the passive silicone model. The major and minor vascular branches were connected at the cranial and caudal ends of the housing through tube ducts and merged with cardiotomy hard-shell reservoirs as compliance chambers for the peripheral upper and lower body vascular compliance and the pulmonary vascular compliance. Adjustable ratios of fluid and air volume allowed the regulation of vascular compliance and volume according to normal cardiovascular function as well as acute heart failure, as previously described.<sup>21</sup> To adjust vascular

**Figure 1** Schematic image of the MCL. CVP, central venous pressure; ECLS, extracorporeal life support; LAP, left-atrial pressure; LVAD, left-ventricular assist device; MAP, mean arterial pressure; MCL, mock circulation loop; PAP, pulmonary arterial pressure; RVAD, right ventricular assist device; VAD, ventricular assist device.



resistance, Hoffman clamps were added to all vascular branches. The major and venous vascular branches were equipped with several antegrade and retrograde large-bore haemostasis valve ports for peripheral and central cannulation. A previously described and validated blood-mimicking fluid for ultrasound studies was used as a blood analogue for the MCL.<sup>18,22</sup> CO was adjusted from the assist device control unit with driving and suction pressure and measured with ultrasound-based transit time clamp-on flow probes

Transonic HXL (Transonic Systems Inc., Ithaca, NY, USA) connected to the vascular branches and corresponding vascular compartments. Blood pressure was measured with clinical strain gauge pressure transducers (Combitrans; Braun, Melsungen, Germany). All pressure levels were continuously recorded with a clinical patient monitor (Intellivue MP 70, Philipps, Hamburg, Germany). For our model, a physiologic CO of 4.0 L/min was defined as the normal condition. To simulate four different stages of low CO syndrome, the

ventricular assist device (VAD) controller settings were modified by reducing the driving and suction pressures and adjusting peripheral resistance of the organ branches with the Hoffman clamps.

To investigate the flow distribution, we assessed the mean blood flow velocity  $V_{\text{mean}}$ , blood flow  $Q_B$  and flow direction, and possible mixing zones using colour-coded Doppler sonography with a linear ultrasound transducer (L12-5 Philips, Hamburg, Germany) connected to a bedside ultrasound system (iE33, Philips, Hamburg, Germany) at 15 regions of interest (ROI) in the aorta and supra-aortic and visceral branches (Figure 2).  $V_{\text{mean}}$  was calculated using the velocity-time integral. Ultrasound coupling was established by filling the PVC housing with sterile body-temperature water as a coupling agent, which allowed direct positioning of the transducer on the selected ROI.

### Measurement of blood flow parameters

The investigation was performed with two cannulation access routes: (i) peripheral femoral (Figure 1A, femoral access) and (ii) central subclavian arterial cannulation (Figure 1B, subclavian access) with a 21 F cannula. Venous cannulation was conducted with a bicaval 23/25 F cannula. The ECLS system consisted of a centrifugal pump (Rotaflow, Getinge, Rastatt, Germany) and a membrane oxygenator (Quadrox, Getinge, Rastatt, Germany).

In the first step, we generated a baseline native CO with corresponding flow, pressure, amplitude ranges, and flow

division in all connected branches, as shown on the left side of Table 1. In the second step, we connected the ECLS system to the MCL and added the corresponding parameters of ECLS flow to achieve the four stages of cardiac failure with pressure ranges and amplitude as well as CO/ECLS flow ratio, as shown on the right side of Table 1.

Within one stage of cardiac failure, we stepwise detected blood flow ( $Q_B$ ), blood flow velocity ( $V_{\text{mean}}$ ), flow vector direction, and the occurrence of mixing zones at the 15 regions in the aorta and its branches (Figure 2). After completion of one series, the MCL was adjusted for the next stage of cardiac depression, and the stepwise measurement started again. The four stages were repeated four times, each with femoral as well as subclavian cannulation, resulting in a total of 32 data sets. The derived values were expressed as the mean  $\pm$  standard deviation. Positive values represent antegrade velocity or flow, whereas negative values represent retrograde velocity or flow. For better discrimination between the different stages of cardiac depression, the results were expressed as linear interpolated line graphs using Originlab 2019 (Additive GmbH, Friedrichsdorf, Germany).

## Results

### System parameter definitions

Four stages of cardiac depression—cardiogenic shock, recovery 1, recovery 2, and weaning—were combined with four

**Figure 2** Schematic drawing of points of measurement in the aortic model.

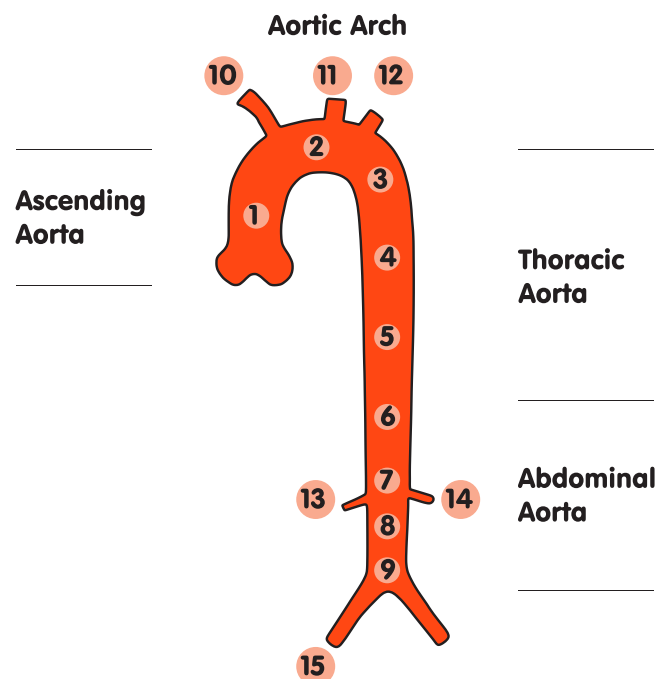


**Table 1** Detailed parameters of the four stages of cardiac depression combined with ECLS

Parameter Scenario	Haemodynamics circulatory system				Cardiac Output total (mL/min)	ECLS		Global haemodynamics	
	MAP (mmHg)	CVP (mmHg)	Flow upper body (mL/min)	Flow lower body (mL/min)		Flow ECLS (mL/min)	Flow ratio CO/ECLS	MAP range (mmHg)	Amplitude (mmHg)
Cardiogenic shock	31 (27–33)	9 (6–11)	200	860	1060	4000	1:4	50–70	0–5
Recovery 1	48 (43–51)	6 (4–7)	1500	520	2020	3000	2:3	60–80	5–15
Recovery 2	61 (58–67)	4 (2–6)	2150	850	3000	2000	3:2	70–90	10–30
Weaning	87 (71–92)	2 (0–3)	840	2400	3240	1000	3:1	70–90	20–50

CO, cardiac output; CVP, central venous pressure; ECLS, extracorporeal life support; MAP, mean arterial pressure. Values are expressed as means with 95% confidence interval.

stages of ECLS flow at a ratio of 1:4–3:1 of native CO to ECLS flow (*Table 1*).

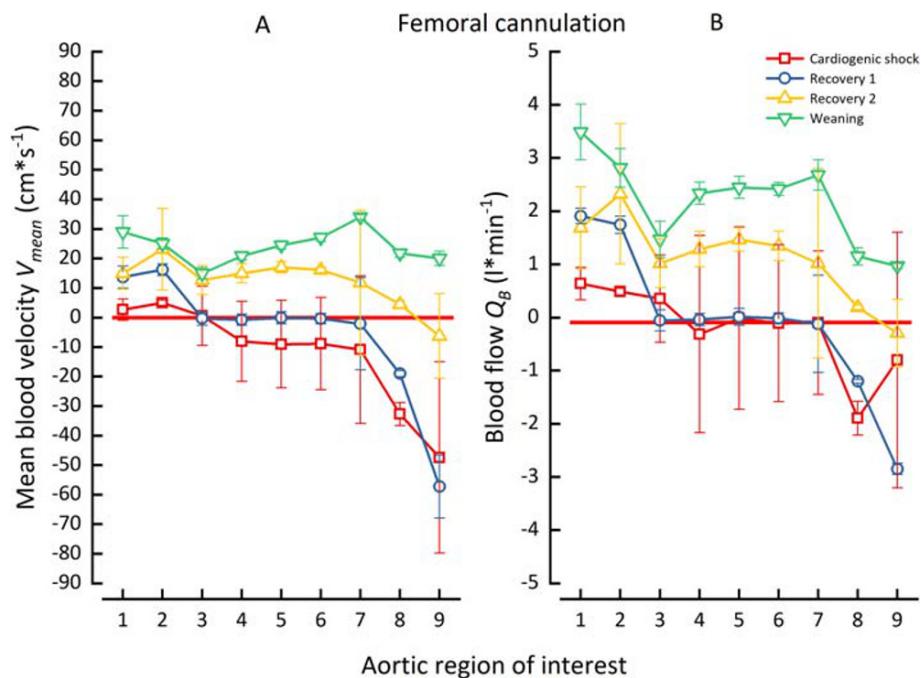
The combination of the baseline haemodynamic parameters of the circulatory system (pressure and flow, *Table 1*, left side) with the additional ECLS flow resulted in higher ranges of mean arterial pressure during all stages of cardiac depression (*Table 1*, right side).

## Blood flow velocity and blood flow in the major arterial tree

### Femoral cannulation

During cardiogenic shock and recovery 1, in which the native circulation was established as 20–40% of the overall flow, an antegrade positive flow could be observed in the ascending aorta and the aortic arch (ROI 1–ROI 2). The corresponding

velocities of these flows in this region were considerably reduced to values lower than 20 cm/s (*Figure 3A*). The stages of cardiogenic shock and recovery 1 showed flows of approximately 0.4 and 1.9 L/min, respectively, which were within the range of the adjusted stages of shock and first recovery (*Figure 3B*). The femoral cannulation led to an expected retrograde flow of the ECLS system beginning in the aortic bifurcation and continuing to the origin of the renal arteries, with high velocities >50 cm/s observed during shock and recovery 1. We detected the formation of a stasis zone with low blood velocities  $\leq 10$  cm/s and a corresponding nearly disappearing flow beginning from the aortic isthmus and continuing to the renal artery origin (ROI 3–ROI 7). This stasis zone was even more pronounced during the stage of first recovery, which had a nearly non-existent velocity and flow (*Figure 3A,B*). The stasis zone thus led to the formation of two watershed zones at the isthmus and the renal artery origin, with a

**Figure 3** Mean blood velocity and blood flow during femoral cannulation.

narrow mixing zone where the opposing flow vectors collided. *Figure 4* shows a watershed at the renal artery origin (ROI 7).

During the recovery 2 and weaning stages, the ECLS flow contributed to an expected normal mean arterial pressure; yet the major part of the overall flow generation was performed by the antegrade-flowing native CO, with nearly normal mean blood flow velocities as well as antegrade flows in all aortic regions. The contribution of the ECLS to the overall flow was thus reduced enormously. As expected, due to flow

distribution within the arterial tree, the flow decreased in distal regions (*Figure 3A,B*).

*Subclavian cannulation*

In contrast to femoral cannulation, the subclavian access led to an antegrade blood flow regardless of the stage of cardiac depression, starting at the isthmus (ROI 3) with a flow decrease in distal regions due to flow distribution (*Figure 5*). The corresponding mean blood velocity was nearly constant at approximately 30–40 cm/s (*Figure 5B*). The brachiocephalic

**Figure 4** Representative image of a watershed during femoral cannulation.

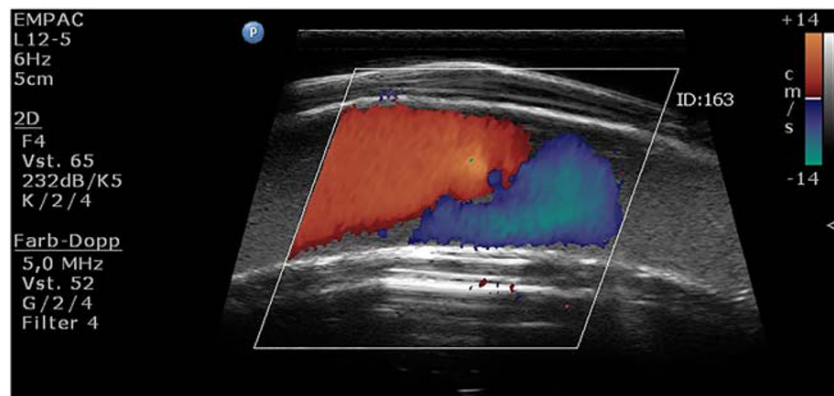
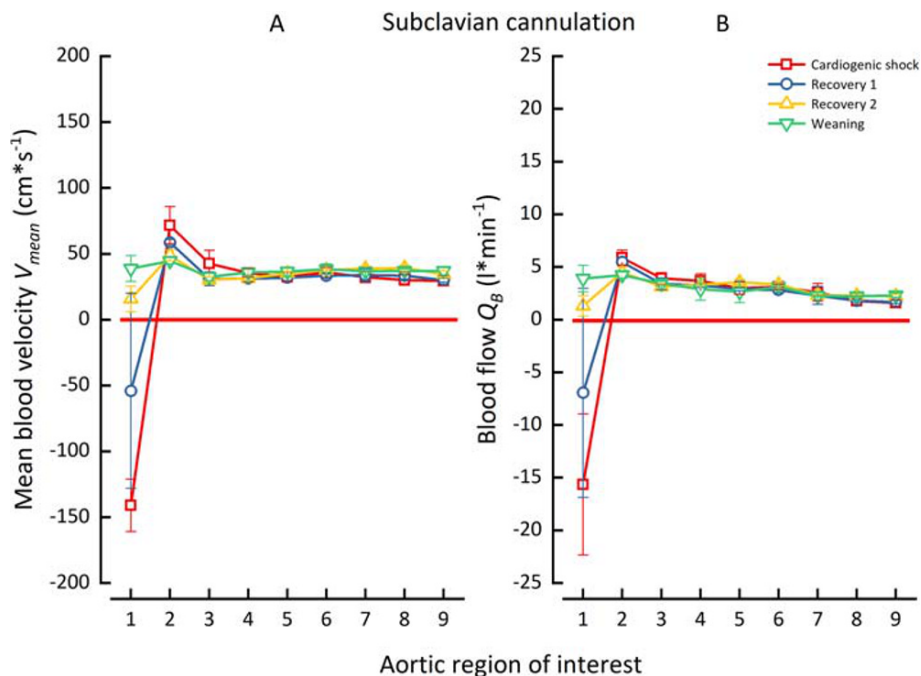


**Figure 5** Mean blood velocity and blood flow during subclavian cannulation.



region (ROI 2) showed higher mean blood velocities at all stages of approximately 50–60 cm/s and higher blood flows due to the proximity of the brachiocephalic outflow of the ECLS flow (Figure 5A,B). The major portion of the antegrade flow arising from the subclavian cannulation was distributed into the aortic arch and more distal parts of the systemic circulation. Notably, there was a massive negative flow vector in the ascending aorta (ROI 1) during cardiogenic shock and recovery 1 with high negative mean blood velocities and corresponding blood flows accompanied by high turbulence, which may explain the high standard deviation. Only during the later stages of recovery 2 and weaning did the negative flow vector transform into positive velocities, accompanied by a corresponding flow in the ascending aorta.

### Blood flow and blood velocity in the supra-aortic and visceral branches

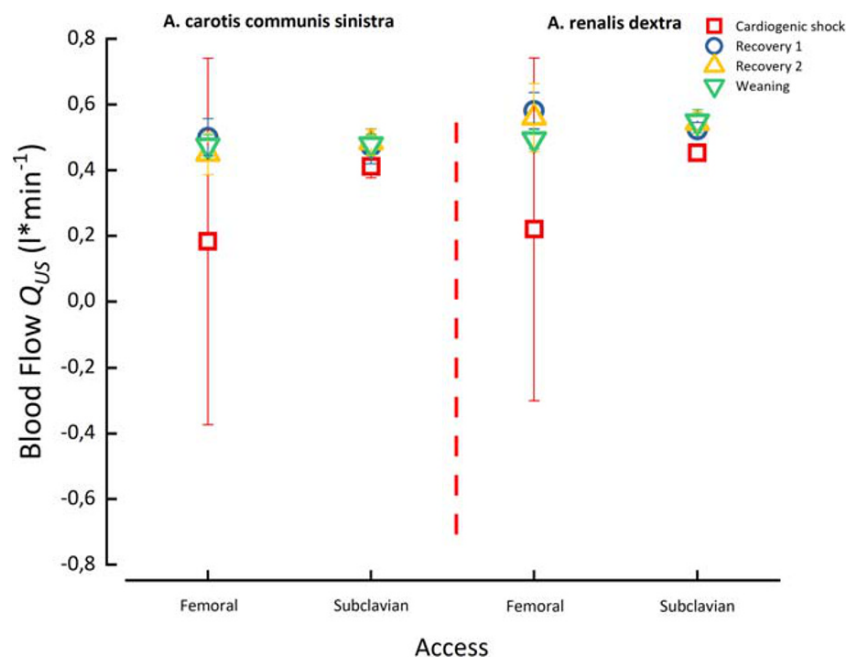
The blood flow during recovery 1, recovery 2, and weaning stages showed a nearly uniform behaviour that was independent of the cannulation access route, with flows of approximately 500 mL/min. Cardiogenic shock resulted in a marked flow decrease of approximately 60%, with flows at 200 mL/min for both cannulation routes, which were accompanied by high turbulence (Figure 6).

## Discussion

The haemodynamic interaction between ECLS and the failing native circulatory system, as two intricately connected and partially opposing sources of flow, plays a pivotal role in critically ill patients. Flow distribution, oxygen delivery to end organs, and left-ventricular unloading may be significant determinants in patient outcomes. In this paper, we demonstrated that ECLS ensured haemodynamic stability but seemed to be incapable of sufficiently distributing blood homogeneously into the end organs of all body regions. In addition to the formation of watersheds, we detected broad zones in the thoracic aorta with reduced blood velocities and nearly no blood flow resulting from a femoral cannulation access route. Although subclavian cannulation resulted in a nearly homogeneous flow distribution during all stages of cardiac depression, the early stages, in particular, resulted in massive negative flow vectors in the ascending aorta, which may increase left-ventricular afterload.

Initial investigations of the impact of ECLS demonstrated that an extracorporeal support system was not able to completely replace the native circulatory system, with its sufficient and homogeneous end-organ supply. Kato demonstrated that arterialized blood does not reach the coronary system during retrograde ECLS.<sup>7</sup> Nowlen confirmed and quantified these findings: during ECLS, the blood supply to the heart and brain decreased by 35–55%.<sup>8</sup> Nowlen and

**Figure 6** Blood flow in the left carotid and right renal artery during femoral and subclavian cannulation.



Smith further confirmed an unequal coronary and cerebral blood supply, as cerebral blood flow seemed to be unaffected by ECLS flow.<sup>8,23</sup> Kinsella reported an important and continuing left-ventricular contribution during ECLS: regardless of ECLS function, up to 90% of the coronary supply was performed by left-ventricular ejection.<sup>11</sup> These results raise the question of whether it is possible to control the flow distribution by ECLS flow adjustment. Secker-Walker showed that an ECLS flow >85% of the overall flow would be required to ensure coronary supply and stated that coronary supply is only possible with a completely absent left-ventricular action.<sup>24</sup> Kamimura later concluded that this flow adjustment would be impossible in reality and would not affect flow distribution.<sup>9</sup> These observational studies have discovered a varying flow distribution within the arterial tree, mainly demonstrated by blood gases and regional flow measurements. The later clinical case series has emphasized the importance of imaging techniques in investigating the location of the separated flow vectors. Hoepfer, Napp, Trummer, and Angleitner used tomography scans and have shown watersheds located between the ascending and descending aorta.<sup>13,15–17</sup> Although Kamimura excluded all controllability, large-scale systematic studies considering the location, flow vectors, distribution of flow, and a possible watershed movement have not yet been conducted. Only Geier has used an artificial aorta model and concentrated on the flow distribution of the supra-aortic branches. A possible movement of the watershed could indirectly be shown by flow distribution changes in the left and right carotid artery.<sup>25</sup>

Our comprehensive MCL approach adds to the current knowledge through a systematic investigation with a high and continuous variability of all haemodynamic boundary conditions. Adding to the work of Geier *et al.*<sup>25</sup> which focussed on an isolated aortic model, we assembled the complete venous and arterial vascular tree with preserved morphological structures, such as ventricles. The pneumatic-driven paracorporeal VADs allowed for the adjustment of all stages of cardiac failure with near-physiological waveforms. Generally, we confirmed an inhomogeneous flow distribution in the major aorta irrespective of the cannulation site, which seemed to be better preserved with subclavian access. Earlier studies have indirectly demonstrated the flow separation with blood gases and flow measurements in specific regions. Our ultrasound approach primarily allows for a confirmation of the watershed at the aortic isthmus, similar to Angleitner.<sup>13</sup> We further showed that the opposing flow vectors during femoral cannulation caused a second watershed at the renal artery origin, which indirectly confirms Alwardts' hypothesis of a broad mixing cloud.<sup>2</sup> Our mixing cloud in the thoracic aorta was limited by two narrow watersheds. More important in this context was the low flow and blood flow velocities within our mixing cloud, which may be prone to sludge formation and thrombus generation. Regarding a possible

movement of the watershed,<sup>13,26</sup> we confirmed Kamimura's earlier conclusion on non-controllability: even during different stages of shock and recovery 1, the watershed at the isthmus region did not show any movement. Efforts to generate a watershed movement by increasing ECLS flow resulted only in a narrowing of the watershed zone, from primarily parabolic-shaped flow vectors to rectangular boundaries. This is important, especially in the first stages of shock and recovery, which may last for several days and thus preserve possible sludge formation.

In contrast, subclavian cannulation led to homogeneous flows and flow distribution in all regions except the ascending aorta. Due to the high blood flow velocities experienced during cardiogenic shock, the negative flow vector prevented an opening of the aortic valve. In addition to sludge formation in the left atrium or ventricle, a non-opening aortic valve may cause left-ventricular distention and a persistent wet lung. Therefore, measures aimed at ventricular unloading seem to be immediately necessary. Venting strategies include placement of a left-atrial venting catheter, atrio-septostomy or antegrade venting using microaxial pumps (e.g. Impella and Abiomed), or intra-aortic balloon counterpulsation. However, according to our data, the placement of an intra-aortic balloon pump in the descending thoracic aorta, where blood stasis is most probable, might increase the risk of thrombus formation.

Although antegrade venting may be required to enhance myocardial recovery, it markedly increases the ejection of deoxygenated blood towards the systemic circulation and favours a compromised coronary and cerebral perfusion. As ventricular unloading with microaxial pumps allowed recovery to begin only after 48 h had passed, the unloading should be adjusted carefully with flows of approximately 600–1000 mL/min to limit the ejection of deoxygenated blood. To further prevent a compromised coronary and cerebral supply, an upgrade from a veno-arterial ECLS to a veno-arterial-venous (VA-V) ECLS, by adding a central venous perfusion cannula to the arterial inflow cannula, may be a therapeutic option<sup>27,28</sup>: the flow separation of the arterial inflow into the arterial and the venous system allows (i) maintenance of haemodynamic stability due to existing extracorporeal flow, (ii) partial pre-pulmonary oxygenation, and (iii) overcoming the inherent flow phenomena of inhomogeneous distribution of oxygenated blood. The mixing of oxygenated blood derived from the extracorporeal system with the venous blood allows an elevated pre-pulmonary oxygen content, a transpulmonary passage, and the ejection of this oxygenated blood into the coronary system. Thus, with this transpulmonary passage, poor coronary perfusion may be prevented.<sup>1,27,29,30</sup> Due to the arterial flow separation, it may be assumed that the mixing of returned oxygenated blood with the venous blood may cause no hyperoxygenation or formation of reactive oxygen species: only a fraction of the entire CO is returned into the venous system and mixes with



an equal or higher fraction of venous blood, resulting in near-normal oxygen saturation.

Although transthoracic or transoesophageal echocardiography are proofed and recommended imaging methods to evaluate the thoracic aorta, they are not fully applicable to completely visualize all parts of the aortic arch and descending aorta.<sup>31</sup> A direct transfer of colour-coded Doppler sonography as used in our experiment is thus limited to visualize watersheds within the arterial tree. We would recommend a multimodal approach to monitor all likely compromised circulatory compartments: to allow assessment of adequate tissue perfusion, blood gas analysis, pulse oximetry, or near-infrared spectroscopy remote from the arterial ECLS access point would show oxygenated blood reaching the supra-aortic or visceral branches and further peripheral tissue. ST-segment abnormalities or arrhythmias would indirectly show poor coronary perfusion caused by compromised pulmonary gas exchange. Echocardiography may primarily be used to assess likely left-ventricular distention. As these methods still do not solve the inhomogeneous distribution of oxygenated blood, an early change to a VA-V ECLS should still play a pivotal role. Of paramount importance for future studies is the likely development of algorithms using surrogate parameters (e.g. flow profiles in accessible regions such as the carotid arteries) to identify the current flow distributions. Measurement of microcirculatory perfusion may be feasible but not measurable by routinely available equipment.

The achieved blood flow ranges in the supra-aortic and visceral branches (left carotid and right renal artery) seemed to be unaffected by later stages of recovery and weaning and were in accordance with previously described reference values of organ blood flow.<sup>32–34</sup> We could only detect flows that were 50% lower than normal and with a high variability during cardiogenic shock. This reduced and non-pulsatile flow may contribute to compromised end-organ function. In conclusion, our ultrasound approach demonstrated an inhomogeneous flow distribution independent of the cannulation access. A persistent and non-shifting broad mixing zone during femoral cannulation may pose a risk of sludge formation, while subclavian cannulation may favour left-ventricular distention.

## Strengths and limitations of the study

### Strengths

#### *Similitude to cardiovascular physiology*

Mock circulatory loops are normally developed for testing VADs and can reproduce stable haemodynamic parameters such as flow, pressure, waveforms, resistance, and compliance. However, their abstracted construction with connecting

pipes, actuators, and chambers, which could mimic the flow processes, does not allow for the detection of flow interactions as it lacks anatomical structures such as the major vascular tree. One strength of our MCL is its preserved anatomical structures, which allow a systematic assessment of flow phenomena including flow direction, flow distribution, and wave phenomena such as watersheds within the vascular tree. In accordance with the similitude theory, which allows a transfer of model data to reality, our MCL fulfils (i) geometrical similarity of the vascular tree regarding shape, size, and mechanical properties, (ii) similarity of the fluid, and (iii) similarity of flow processes.<sup>22,30,35,36</sup>

#### *Stability of mock circulation loop parameters*

With the preset pressures of the paracorporeal VADs and the resistive and capacitive elements, the MCL showed stable behaviour within 1 h without any significant volume shifts between the body compartments and the systemic and pulmonary loop. Repeated shut down manoeuvres with resulting fluid and pressure equilibrium of the MCL allowed reproducible parameters within 10 min with continued stability. The reproduction of the several stages of cardiac depression required a sole adjustment of the driving pressures of the VADs without any changes in the preset resistive and capacitive parameters.<sup>18</sup>

### Limitations

#### *Anatomical limitations*

It should be noted that the lack of surrounding soft tissue within the MCL and the lack of a coronary system may have changed compliance, pulse wave propagation, and overall flow distribution. However, during validation, the near-physiologic changes of pressures and waveforms of the MCL during all stages of cardiac depression were in accordance with the published clinical stages of heart failure.<sup>37</sup>

#### *Lack of feedback mechanism*

The implementation of feedback mechanisms such as the baroreceptor control would have resulted in higher haemodynamic stability, but we focussed on reproducible and stable stages of cardiac failure.

#### *Passive silicone ventricle*

The passive non-contracting silicone ventricle may have changed the watershed location due to the lack of pulsatile ejection. However, with the blood pressure cuff wrapped around the left ventricle, we were able to reproduce ejection fractions around 10% that are similar to a cardiogenic shock.<sup>38</sup>

#### *Ultrasound parameters*

The use of water as tissue-mimicking material was a necessary compromise to allow recurrent assembly, filling, and

de-airing of all MCL components during operation. Its acoustic velocity of 1470 m/s is close to the acoustic velocity of soft tissue (1540–1570 m/s) as previously described.<sup>39</sup> This would have been impossible with other tissue-mimicking materials such as agar gels or foam, which are used for ultrasound phantoms.<sup>40</sup> Silicone, as vessel material, despite its high acoustic attenuation, has been used by several authors for ultrasound flow phantoms.<sup>41,42</sup> The use of blood-mimicking fluid has been previously tested in accordance with International Electrotechnical Commission requirements for flow phantoms.<sup>40</sup>

### Doppler velocity measurement

Due to an incorrect adjustment of the probe to vessel angle and inaccurate positioning of the sample volume within the vessel, the estimation of velocity derived through the velocity-time integral may be biased. Lui reported an overestimation of the true peak velocity of a carotid flow phantom: in a straight and stenosed carotid artery model, the peak velocity was 8–16% and 7–28% higher than the true peak velocity.<sup>43</sup> It may cautiously be assumed that our calculated mean blood velocity was higher than the true velocity within our vascular tree. This only affects the velocity estimation but not the location of our detected watersheds, which seemed to be in accordance with the clinical context of watershed formation.<sup>2,13,14,16,17,30</sup>

## Conclusion

Compromised end-organ supply with likely deoxygenated blood, large aortic stasis zones, and unsolved left-ventricular distention are clinical entities that are not easily identified by conventional bedside methods. Apparent haemodynamic stability during ECLS may thus give a false sense of security.

## References

- Napp LC, Kühn C, Hoepfer MM, Vogel-Claussen J, Haverich A, Schäfer A, Bauersachs J. Cannulation strategies for percutaneous extracorporeal membrane oxygenation in adults. *Clin Res Cardiol* 2016; **105**: 283–296.
- Alwardt CM, Patel BM, Lowell A, Dobberpuhl J, Riley JB, DeValeria PA. Regional perfusion during venoarterial extracorporeal membrane oxygenation: a case report and educational modules on the concept of dual circulations. *J Extra Corpor Technol* 2013; **45**: 187–194.
- Burkhoff D, Sayer G, Doshi D, Uriel N. Hemodynamics of mechanical circulatory support. *J Am Coll Cardiol* 2015; **66**: 2663–2674.
- Prasad A, Ghodsizad A, Brehm C, Kozak M, Körner M, El Banayosy A, Singbartl K. Refractory pulmonary edema and upper body hypoxemia during veno-arterial extracorporeal membrane oxygenation—a case for atrial septostomy. *Artif Organs* 2018; **42**: 664–669.
- Tepper S, Masood MF, Baltazar Garcia M, Pisani M, Ewald GA, Lasala JM, Bach RG, Singh J, Balsara KR, Itoh A. Left ventricular unloading by impella device versus surgical vent during extracorporeal life support. *Ann Thorac Surg* 2017; **104**: 861–867.
- Napp LC, Kühn C, Bauersachs J. ECMO in cardiac arrest and cardiogenic shock. *Herz* 2017; **42**: 27–44.
- Kato J, Seo T, Ando H, Takagi H, Ito T. Coronary arterial perfusion during venoarterial extracorporeal membrane oxygenation. *J Thorac Cardiovasc Surg* 1996; **111**: 630–636.
- Nowlen TT, Salley SO, Whittlesey GC, Kundu SK, Maniaci NA, Henry RL, Klein MD. Regional blood flow distribution during extracorporeal membrane oxygenation in rabbits. *J Thorac Cardiovasc Surg* 1989; **98**: 1138–1143.
- Kamimura T, Sakamoto H, Misumi K. Regional blood flow distribution from the proximal arterial cannula during veno-arterial extracorporeal membrane oxygenation in neonatal dog. *J Vet Med Sci* 1999; **61**: 311–315.

Although ECLS restores haemodynamic stability, our findings demonstrate that different cannulation access routes still do not solve the inherent flow separation phenomenon, which likely influences mortality and morbidity. An obviously non-controllable watershed provokes the clinician to apply new cannulation strategies such as the VA-V ECLS, which delivers oxygenated blood into the arterial and venous vascular bed for improved end-organ supply. The common references to these problems in small clinical observations and case studies are confirmed by this systematic *in vitro* investigation.

## Conflict of interest

Andreas Böning and Philippe Grieshaber received research support from The German Heart Foundation, the University Hospital Giessen and Marburg Research Fund, and the von-Behring-Röntgen Foundation. Andreas Böning received presentation honoraria from Abbott Zoll, Bayer, B. Braun Maquet, Smith & Nephew, Somahlution, and Spectranetics. Johannes Gehron received presentation honoraria from Getinge Deutschland GmbH, Keller Medical GmbH, and Terumo Deutschland GmbH. Philippe Grieshaber received a travel grant from Orion Pharma GmbH, Hamburg. Markus Bongert, Martin Fiebich, Gabriele Krombach, Florian Rindler, and Maximilian Schuster declare that they have no conflict of interest.

## Funding

This work was supported by the von-Behring-Röntgen-Foundation. The aortic valve prosthesis used in this study was provided free of cost by Medtronic, Luxembourg.

10. Wada H, Watari M, Sueda T, Kochi K, Sakai H, Shibamura H, Imai K, Fukunaga S, Orihashi K, Matsuura Y. Cerebral tissue oxygen saturation during percutaneous cardiopulmonary support in a canine model of respiratory failure. *Artif Organs* 2000; **24**: 640–643.
11. Kinsella JP, Gerstmann DR, Rosenberg AA. The effect of extracorporeal membrane oxygenation on coronary perfusion and regional blood flow distribution. *Pediatr Res* 1992; **31**: 80–84.
12. Nakamura T, Takata M, Arai M, Nakagawa S, Miyasaka K. The effect of left-to-right shunting on coronary oxygenation during extracorporeal membrane oxygenation. *J Pediatr Surg* 1999; **34**: 981–985.
13. Angleitner P, Roggla M, Laufer G, Wiedemann D. Watershed of veno-arterial extracorporeal life support. *Eur J Cardiothorac Surg* 2016; **50**: 785.
14. Avgerinos DV, DeBois W, Voevidko L, Salemi A. Regional variation in arterial saturation and oxygen delivery during venoarterial extracorporeal membrane oxygenation. *J Extra Corpor Technol* 2013; **45**: 183–186.
15. Hoepfer MM, Tudorache I, Kühn C, Marsch G, Hartung D, Wiesner O, Boenisch O, Haverich A, Hinrichs J. Extracorporeal membrane oxygenation watershed. *Circulation* 2014; **130**: 864–865.
16. Napp LC, Brehm M, Kühn C, Schäfer A, Bauersachs J. Heart against veno-arterial ECMO: competition visualized. *Int J Cardiol* 2015; **187**: 164–165.
17. Trummer G, Benk C, Heilmann C, Beyersdorf F. Visualization of hypoxemic coronary perfusion despite full retrograde extracorporeal circulatory life support. *Eur J Cardiothorac Surg* 2013; **43**: e47.
18. Gehron J, Zirbes J, Bongert M, Schäfer S, Fiebich M, Krombach G, Böning A, Grieshaber P. Development and validation of a life-sized mock circulatory loop of the human circulation for fluid-mechanical studies. *ASAIO J* 2019; **65**: 788–797.
19. Lang RM, Cholley BP, Korcarz C, Marcus RH, Shroff SG. Measurement of regional elastic properties of the human aorta. A new application of transesophageal echocardiography with automated border detection and calibrated subclavian pulse tracings. *Circulation* 1994; **90**: 1875–1882.
20. Stefanadis C, Stratos C, Vlachopoulos C, Marakas S, Boudoulas H, Kallikazaros I, Tsiamis E, Toutouzas K, Sioros L, Toutouzas P. Pressure-diameter relation of the human aorta. A new method of determination by the application of a special ultrasonic dimension catheter. *Circulation* 1995; **92**: 2210–2219.
21. Knierbein B, Reul H, Eilers R, Lange M, Kaufmann R, Rau G. Compact mock loops of the systemic and pulmonary circulation for blood pump testing. *Int J Artif Organs* 1992; **15**: 40–48.
22. Ramnarine KV, Nassiri DK, Hoskins PR, Lubbers J. Validation of a new blood-mimicking fluid for use in Doppler flow test objects. *Ultrasound Med Biol* 1998; **24**: 451–459.
23. Smith HG, Whittlesey GC, Kundu SK, Salley SO, Kuhns LR, Chang CH, Klein MD. Regional blood flow during extracorporeal membrane oxygenation in lambs. *ASAIO Trans* 1989; **35**: 657–660.
24. Secker-Walker JS, Edmonds JF, Spratt EH, Conn AW. The source of coronary perfusion during partial bypass for extracorporeal membrane oxygenation (ECMO). *Ann Thorac Surg* 1976; **21**: 138–143.
25. Geier A, Kunert A, Albrecht G, Liebold A, Hoenicka M. Influence of cannulation site on carotid perfusion during extracorporeal membrane oxygenation in a compliant human aortic model. *Ann Biomed Eng* 2017; **45**: 2281–2297.
26. Napp LC, Schmitto JD, Tongers J, Schäfer A. The short- and long-term risks of venoarterial extracorporeal membrane oxygenation watershed. *Eur J Cardiothorac Surg* 2017; **53**: 894–894.
27. Brand M, Christ M, Dierschke W, Amirie S, Roeing J, Grett M, Beko M, Breker I, Wennemann R, Trappe H-J. Erweiterung einer venoarteriellen (VA) ECMO auf eine venovenarterielle (VVA) ECMO bei schwerem Harlekinsyndrom. *Der Kardiologe* 2017; **11**: 121–124.
28. Broman LM, Taccone FS, Lorusso R, Malferteiner MV, Pappalardo F, Di Nardo M, Belliato M, Bembea MM, Barbaro RP, Diaz R, Grazioli L, Pellegrino V, Mendonca MH, Brodie D, Fan E, Bartlett RH, McMullan MM, Conrad SA. The ELSO Maastricht Treaty for ECLS Nomenclature: abbreviations for cannulation configuration in extracorporeal life support—a position paper of the Extracorporeal Life Support Organization. *Crit Care* 2019; **23**: 36.
29. Brasseur A, Scolletta S, Lorusso R, Taccone FS. Hybrid extracorporeal membrane oxygenation. *J Thorac Dis* 2018; **10**: S707–S715.
30. Guihaire J, Haddad F, Hoppenfeld M, Amsallem M, Christle JW, Owyang C, Shaikh K, Hsu JL. Physiology of the assisted circulation in cardiogenic shock: a state-of-the-art perspective. *Can J Cardiol* 2020; **36**: 170–183.
31. Goldstein SA, Evangelista A, Abbara S, Arai A, Asch FM, Badano LP, Bolen MA, Connolly HM, Cuellar-Calabria H, Czerny M, Devereux RB, Erbel RA, Fattori R, Isselbacher EM, Lindsay JM, McCulloch M, Michelena HI, Nienaber CA, Oh JK, Pepi M, Taylor AJ, Weinsaft JW, Zamorano JL, Dietz H, Eagle K, Eleftheriades J, Jondeau G, Rousseau H, Schepens M. Multimodality imaging of diseases of the thoracic aorta in adults: from the American Society of Echocardiography and the European Association of Cardiovascular Imaging: endorsed by the Society of Cardiovascular Computed Tomography and Society for Cardiovascular Magnetic Resonance. *J Am Soc Echocardiogr* 2015; **28**: 119–182.
32. Garcia J, van der Palen RLF, Bollache E, Jarvis K, Rose MJ, Barker AJ, Collins JD, Carr JC, Robinson J, Rigsby CK, Markl M. Distribution of blood flow velocity in the normal aorta: effect of age and gender. *J Magn Reson Imaging* 2018; **47**: 487–498.
33. Nichols WW, Nichols WW, McDonald DA. *McDonald's blood flow in arteries: theoretic, experimental, and clinical principles*, 6th ed. London: Hodder Arnold; 2011.
34. Williams LR, Leggett RW. Reference values for resting blood flow to organs of man. *Clin Phys Physiol Meas* 1989; **10**: 187–217.
35. Reul H, Tesch B, Schoenmackers J, Effert S. Hydromechanical simulation of systemic circulation. *Med Biol Eng* 1974; **12**: 431–436.
36. Sharp MK. Models of the cardiovascular system. In Shrivastava D., ed. *Theory and Applications of Heat Transfer in Humans*. New York, NY: Wiley; 2018. p 71–118.
37. Ponikowski P, Voors AA, Anker SD, Bueno H, Cleland JGF, Coats AJS, Falk V, González-Juanatey JR, Harjola V-P, Jankowska EA, Jessup M, Linde C, Nihoyannopoulos P, Parissis JT, Pieske B, Riley JP, Rosano GMC, Ruilope LM, Ruschitzka F, Rutten FH, van der Meer P, Group ESC. 2016 ESC Guidelines for the diagnosis and treatment of acute and chronic heart failure: The Task Force for the diagnosis and treatment of acute and chronic heart failure of the European Society of Cardiology (ESC) Developed with the special contribution of the Heart Failure Association (HFA) of the ESC. *Eur Heart J* 2016; **37**: 2129–2200.
38. Barth T, Grieshaber P, Bongert M, Böning A, Fiebich M, Krombach G, Dahm M, Gehron J. Evaluierung eines Silikonventrikels in einem Herz-Kreislaufsimulator mittels Echokardiographie. *Kardiotechnik* 2018; **27**: 66–73.
39. Benedetto G, Gaviolo RM, Albo PAG, Lago S, Ripa DM, Spagnolo R. Speed of sound in pure water at temperatures between 274 and 394 K and at pressures up to 90 MPa. *Int J Thermophys* 2005; **26**: 1667–1680.
40. Hoskins PR. Simulation and validation of arterial ultrasound imaging and blood flow. *Ultrasound Med Biol* 2008; **34**: 693–717.

41. Holmes D, Rettmann M, Cameron B, Camp J, Robb R. *Developing patient-specific anatomic models for validation of cardiac ablation guidance procedures*. SPIE; 2008.
42. McLeod AJ, Moore J, Lang P, Bainbridge D, Campbell G, Jones D, Guiraudon G, Peters T. *Evaluation of Mitral Valve Replacement Anchoring in a Phantom*. SPIE; 2012.
43. Lui EY, Steinman AH, Cobbold RS, Johnston KW. Human factors as a source of error in peak Doppler velocity measurement. *J Vasc Surg* 2005; **42**: 972–979.